Environmental Science and Pollution Research (2023) 30:59737–59748
https://doi.org/10.1007/s11356-023-26740-9

RESEARCH ARTICLE

Construction of 3D sheet-packed hierarchical MoS_2/BiOBr heterostructures with remarkably enhanced photocatalytic performance for tetracycline and levofloxacin degradation

Zhanying Ma[1] · Xiaobo Li[1] · Guang Fan[1] · Lingjuan Deng[1] · Yangqing He[2]

Received: 24 October 2022 / Accepted: 27 March 2023 / Published online: 4 April 2023

Abstract

In this paper, MoS_2 nanosheets were prepared and deposited on BiOBr microflowers through deposition-hydrothermal strategy. MoS_2 exhibited a string of nanosheets with wrinkled layer outlook, and MoS_2/BiOBr composites displayed a micro-flower morphology with the diameter of 2-3 μm. Visible-light harvesting performance was significantly improved in the region of 400-600 nm for MoS_2/BiOBr. The obtained MoS_2/BiOBr samples exhibited tremendous enhanced catalytic activity, which could degrade 92.96% of tetracycline and 90.31% of levofloxacin within 70 min. The photo-generated holes and ·OH radicals played the dominant roles in the whole photocatalytic decomposition process. Based on the analysis of DRS, BET, PL, and electrochemical results, the remarkably improved photocatalytic performance may be ascribed to the synergistic effect of strong visible-light harvesting ability, enhanced BET surface area, and faster separation or transfer efficiency of photo-generated charges.

Keywords MoS_2/BiOBr · Photocatalysis · Antibiotic residue removal · Heterojunctions

Introduction

In the last two decades, antibiotic residues were inevitably discharged into various water bodies since the antibiotics were enormously produced and extensively used for medical therapy because of its excellent activity against bacterial infection (Li et al. 2019a; Hu et al. 2021). Antibiotics polluted wastewater would provoke potential threats to the public health and ecosystem due to its toxic nature. Therefore, it is urgent to explore an efficient technology to eliminate the antibiotic residues before discharge. Among various wastewater treatment techniques, semiconductor photocatalysis has been considered as an effective approach to remove antibiotics pollutants due to its non-toxicity, cost-effective, and ambient operating condition (Chen et al. 2019; Pirhashemi et al. 2018; Sabri et al. 2021).

Bismuth oxybromide (BiOBr) is a V-VI-VII ternary oxide semiconductor material with layered tetragonal matlockite structure. The $[Bi_2O_2]^{2+}$ positive slices were embedded in double Br negative slabs to yield [Br-Bi-O-Bi-O-Br] layers (Xu et al. 2014). Then [Br-Bi-O-Bi-O-Br] layers interacted together through van der Waals forces rather than closely packed, resulting in larger BET surface area and ideal absorption abilities (Xiong et al. 2014). As reported, BiOBr has been evidenced as a promising visible-light-induced photocatalyst to decompose organic effluents due to its high stability against photocorrosion, appropriate band gap (1.7-3.2 eV), and relatively excellent photocatalytic performance (Xue et al. 2014, Mao et al. 2014). Nevertheless, the low separation efficiency of photo-generated electron/hole pairs severely hindered its practical applications. Previous investigations had specified that coupling BiOBr and another semiconductor with suitable band gap to form heterojunction was an efficient strategy to promote separation rate of charge carriers (Meng and Zhang 2015; Wang et al. 2014). Up to now, various BiOBr-based heterojunctions with improved photocatalytic activities had been extensively investigated,

Responsible Editor: Sami Rtimi

✉ Yangqing He
yqhe6@xaut.edu.cn

[1] Department of Chemistry, Xianyang Normal University, Xianyang 712000, China

[2] Department of Applied Chemistry, Xi'an University of Technology, Xi'an 710048, China

such as BiOAc/BiOBr (Liu et al. 2021), BiOBr/$BiFeWO_6$ (Lu et al. 2021), BiOBr/BiOCl (Liao et al. 2021), $BiSbO_4$/BiOBr (Van et al. 2022), BiOBr/C_3N_4 (Ma et al. 2019a), and so on. The outstanding degradation performance of these photocatalysts depended on their preferable optical-absorption characteristics, high separation efficiency of excited charge carriers and long-term stability.

Molybdenum disulfide (MoS_2) has a similar layered structure to BiOBr, in which Mo atoms were sandwiched covalently between S atoms to form S-Mo-S layers. Then, each formed S-Mo-S layer vertically connected together by van Der Waals interactions, which facilitated the exfoliation of 2D MoS_2 nanosheets from bulk MoS_2. This typical layered structure not only significantly improved the utilization of active center but also greatly shortened the transfer path of photo-induced charge carriers, degradation intermediates, and products. Other excellent properties of MoS_2 includes its light absorption performance (Eg = 1.2-1.9 eV), unique physical and chemical performance, and stability against photo-corrosion. Therefore, MoS_2 was used as an ideal co-catalyst to modify C_3N_4 (Li et al. 2019b; Akhundi et al. 2020), CdS (Darsara et al. 2018), Bi_2S_3 (Iqbal et al. 2022), ZnO (Benavente et al. 2018), Bi_2O_3 (Ma et al. 2019b), and the obtained composites showed the improved photocatalytic performance for degradation organic pollutants. Significant investigations of BiOBr/MoS_2 heterojunctions have been documented for eliminating organic dyes (Zhang et al. 2021; Lee et al. 2017), where the conduction band potential was higher than that of BiOBr, and type-I band alignment was formed at BiOBr/MoS_2 interface. It promoted the charge separation and further enhanced the photocatalytic activity. The photocatalytic performance of BiOBr modified with MoS_2 also depended on the layer number in MoS_2 and the weight percentage of MoS_2 deposited on BiOBr.

Considering the unique properties of few-layered MoS_2, in this work, few-layered MoS_2 nanosheets were fabricated firstly by a simple hydrothermal-dialysis method, and then deposited on the surface of BiOBr microflowers via a deposition-hydrothermal process. As a result, few-layer MoS_2 nanosheets coupled with BiOBr heterojunctions were successfully fabricated. The visible-light absorption capacity was enhanced, and the separation or transfer efficiency of excited charge carriers was remarkably promoted. The photocatalytic performance of as-synthesized MoS_2/BiOBr microflowers was evaluated by degradation of tetracycline and levofloxacin antibiotics. The detailed relationship between the unique structure and the excellent catalytic performance of MoS_2/BiOBr microflowers was explored. The possible enhanced photocatalytic mechanism was also proposed based on various experimental investigations. Furthermore, this fabrication method could be extended into a general strategy for the formation of other 2D few-layered heterojunctions.

Experimental

Materials

Sodium molybdate [Na_2MoO_4], thiourea [CH_4N_2S], bismuth nitrate pentahydrate [$Bi(NO_3)_3{\cdot}5H_2O$], cetyltrimethylammonium bromide (CTAB), anhydrous ethanol (EtOH), tetracycline, and levofloxacin were used without further purification.

Preparation of MoS_2 nanosheets

About 0.6 g of Na_2MoO_4 was dissolved in deionized water with continuous ultrasonication for 10 min to obtain the transparent Na_2MoO_4 solution, followed by the addition of CH_4N_2S (0.5 g). The as-obtained mixture solution was migrated into a 50-mL Teflon-lined stainless steel autoclave and kept at 190 °C for 24 h to get MoS_2 suspension. After centrifuge at 10,000 rpm for 10 min, the supernatant was transferred to a dialysis bag and kept on dialysis for 2 days. Finally, MoS_2 nanosheet dispersion was obtained for the following step.

Preparation of MoS_2/BiOBr heterojunctions

The MoS_2/BiOBr heterojunctions were prepared via a simple deposition-hydrothermal method. Typically, 0.729 g of CTAB was dissolved in a specified amount of anhydrous ethanol, followed by the addition of bismuth nitrate pentahydrate (0.9702 g). After ultrasonication for 30 min, 4 mL of MoS_2 nanosheets dispersion was added. The obtained suspension was added into a 100-mL Teflon-lined stainless-steel autoclave and heated for 17 h at 160 °C. The product was cooled down to 25 °C and separated by filtration. The obtained precipitate was washed with anhydrous ethanol and dried at 60 °C to obtain MoS_2/BiOBr samples, marked as 4-MoS_2/BiOBr. Pure BiOBr was also synthesized using the similar procedure without the addition of MoS_2 nanosheet dispersion. By changing the volume amounts of MoS_2 nanosheet dispersion, 6-MoS_2/BiOBr, 8-MoS_2/BiOBr, and 10-MoS_2/BiOBr samples were also prepared with other parameters unchanged for comparison.

Characterization of the prepared samples

Crystal structure was studied by X-ray diffractometer (D8 ADVANCE A25, Cu Kα, λ = 1.54056 Å). The morphology was investigated by scanning electron microscopy (S-3000N) and field emission transmission electron microscopy (G2F30). The surface chemical state was detected using X-ray photoelectron spectroscope (AXIS ULtrabld),

operating at 3.0×10^{-10} mbar. The optical absorption property was investigated by Lambd 950 UV-visible diffuse reflectance spectrophotometer. The photoluminescence spectra were measured using RF-6000 Fluorescence spectrophotometer.

Photocatalytic experiment

Photocatalytic capability of the samples was evaluated by elimination of tetracycline and levofloxacin antibiotics. The detailed process was described in our previous work (Ma et al. 2019a). In a typical process, under the dark condition, 10 mg of the samples was applied to degrade 40 mL tetracycline (20 mg/L) or levofloxacin (20 mg/L) solution with vigorous stirring for 20 min to obtain the equilibrium of adsorption/desorption. Then, the dispersion was continuously irradiated with a 250 W Xe lamp. Also, 4 mL suspension was sequentially collected at each 10 min interval and centrifuged through membrane filters (0.22 μm) to take away the solid photocatalyst. The obtained filtrate was transferred into a quartz cuvette to investigate the absorption spectra (200-750 nm) using a UV-3200 spectrophotometer.

The long-term stability was studied as follows. 6-MoS_2/BiOBr heterojunctions were recycled through centrifugation after the degradation of tetracycline and levofloxacin, respectively, then rinsed with deionized water and recycled to another run.

Results and discussion

Crystal phase structure analysis

The XRD patterns of BiOBr, MoS_2, and MoS_2/BiOBr composites (4-MoS_2/BiOBr, 6-MoS_2/BiOBr, 8-MoS_2/BiOBr, and 10-MoS_2/BiOBr) are displayed in Fig. 1. For BiOBr sample, the main detected peaks could be well indexed to (001), (002), (101), (102), (110), (112), (200), and (212) planes of tetragonal phase structure (JCPDS No. 09-0393). The diffraction signals of MoS_2 were assigned to (002), (100), and (110) planes of the hexagonal phase (Chandrabose et al. 2021). While for MoS_2/BiOBr composites, all detected peaks were well matched to tetragonal BiOBr, and no distinct diffraction peaks of MoS_2 were observed because the content of MoS_2 was too low to detect.

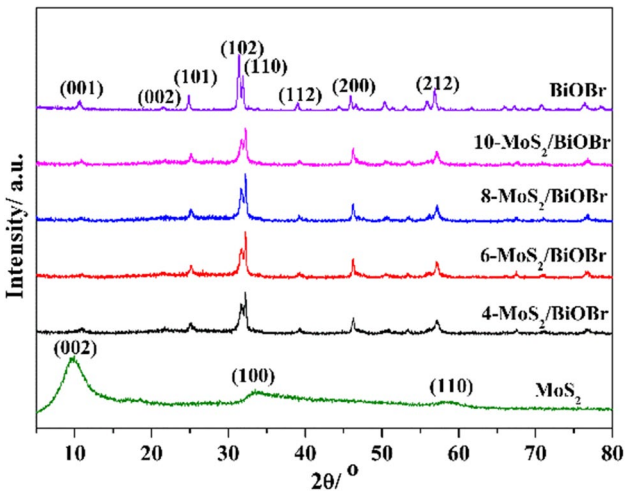

Fig. 1 XRD patterns of BiOBr, MoS_2, and MoS_2/BiOBr composites

Morphology analysis

The morphology, size, and lattice were characterized by SEM, TEM, and HRTEM techniques. The results are shown in Fig. 2. From Fig. 2 a, it is clearly observed that MoS_2 shows accumulated states of thin nanoplates with the smooth surface. The TEM in Fig. 2 b displays that MoS_2 exhibits a string of nanosheets with a wrinkled layer outlook and sufficient exposed edges, further confirming the thin size and smooth surface of MoS_2 nanosheet. The 0.947-nm lattice spacing in the HRTEM of MoS_2 (Fig. 2c) could be indexed to its (002) facet (Hu et al. 2020). Figure 2 d indicates that 6-MoS_2/BiOBr composites have a micro-flower morphology, with the diameter of 2~3 μm, fabricated by some interlaced nanosheets with a thickness of 35 nm. The enlarged SEM (inset of Fig. 2d) further indicated that 6-MoS_2/BiOBr micro-flowers were self-assembled by numerous BiOBr nanosheets and MoS_2 nanoplates (marked by yellow arrow) were attached on the surface of BiOBr. The TEM images as shown in Fig. 2 e confirm the as-prepared 6-MoS_2/BiOBr are sheet-packed 3D hierarchical structures. To confirm the formation of heterojunction between MoS_2 and BiOBr in 6-MoS_2/BiOBr composites, HRTEM technique is employed, and the results are shown in Fig. 2 f. An obvious tight contact boundary (marked by a yellow line) between MoS_2 and BiOBr was evidently observed, which proved that MoS_2 was closely attached to the BiOBr microstructure. It facilitated the charge separation during photocatalytic degradation process (Liu et al. 2018). Notably, clear lattice fringes with a spacing of 0.278 and 0.282 nm were obvious, which could be ascribed to (102) and (110) facet of BiOBr.

Figure 3 is the elemental mapping results of 6-MoS_2/BiOBr composites. The Bi, Br, O, Mo, and S elements were distributed in the selected district and had a good synergistic correspondence with the whole scanning region, indicating that MoS_2 were attached or immersed well into BiOBr microstructure. This result further proved that MoS_2/BiOBr composites were successfully prepared.

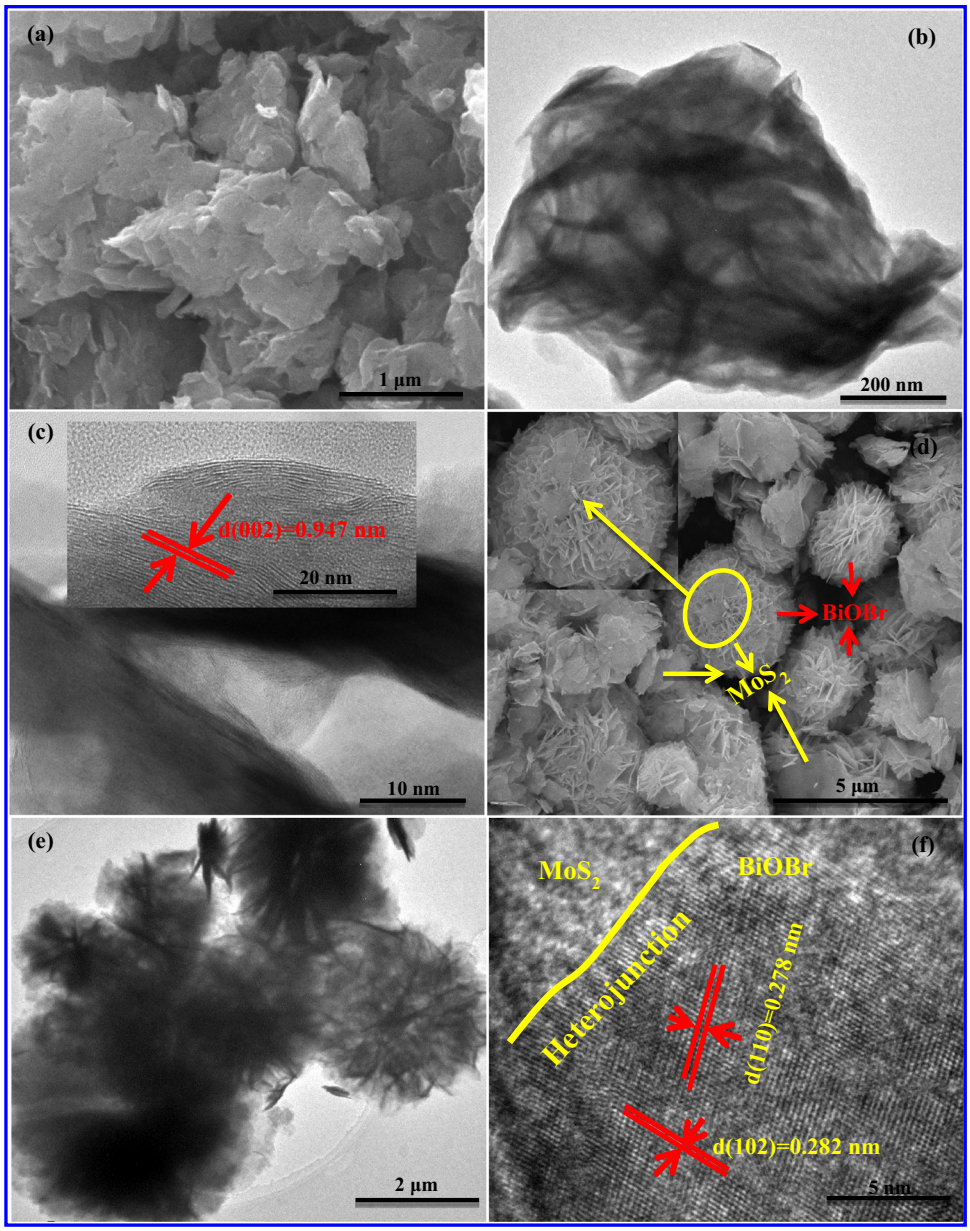

Fig. 2 SEM images of MoS_2 (**a**) and 6-MoS_2/BiOBr composites (**d**), TEM images of MoS_2 (**b**) and 6-MoS_2/BiOBr composites (**e**), and HRTEM images of MoS_2 (**c**) and 6-MoS_2/BiOBr composites (**f**)

XPS analysis

To further prove the interaction between MoS_2 and BiOBr in the heterojunctions and explore the chemical states of 6-MoS_2/BiOBr, X-ray photoelectron spectroscopies (XPS) are carried out, and the results are shown in Fig. 4. Figure 4 a shows the full spectra of BiOBr and 6-MoS_2/BiOBr. Bi, O, and Br elements could be observed in the spectrum of BiOBr. From the spectrum of 6-MoS_2/BiOBr, Mo, and S elements were detected in addition to Bi, O, and Br, implying the successful synthesis of 6-MoS_2/BiOBr. Figure 4 b–f are the XPS high resolution spectra of Mo 3d, S 2p, Bi 4f, O 1s, and Br 3d. From Fig. 4 b, the two strong Mo 3d signals at 235.53 and 232.29 eV could be ascribed to Mo $3d_{3/2}$ and Mo $3d_{5/2}$, respectively, demonstrating the valence of molybdenum in 6-MoS_2/BiOBr sample was +4. The XPS peaks at 164.56 and 159.2 eV shown in Fig. 4 c could be attributed to S $2p_{1/2}$ and S $2p_{3/2}$ (Li et al. 2018). From Fig. 4 d, two peaks at 164.4 and 159.1 eV for BiOBr sample corresponding to Bi $4f_{5/2}$ and Bi $4f_{7/2}$ are shifted to higher binding energies by 0.1 and 0.16 eV for 6-MoS_2/BiOBr sample, respectively. The O 1s signal at 529.9 eV of BiOBr in Fig. 4 e could be ascribed to Bi–O bond (Li et al. 2023), which was shifted to 530.1 eV with apparent decreased intensity owning to the coupling of MoS_2 in 6-MoS_2/BiOBr sample. Two signals with binding energies at 69.13 and 68.24 eV presented for pure BiOBr belonging to Br $3d_{3/2}$ and Br $3d_{5/2}$ were shifted to 69.31 and 68. 4

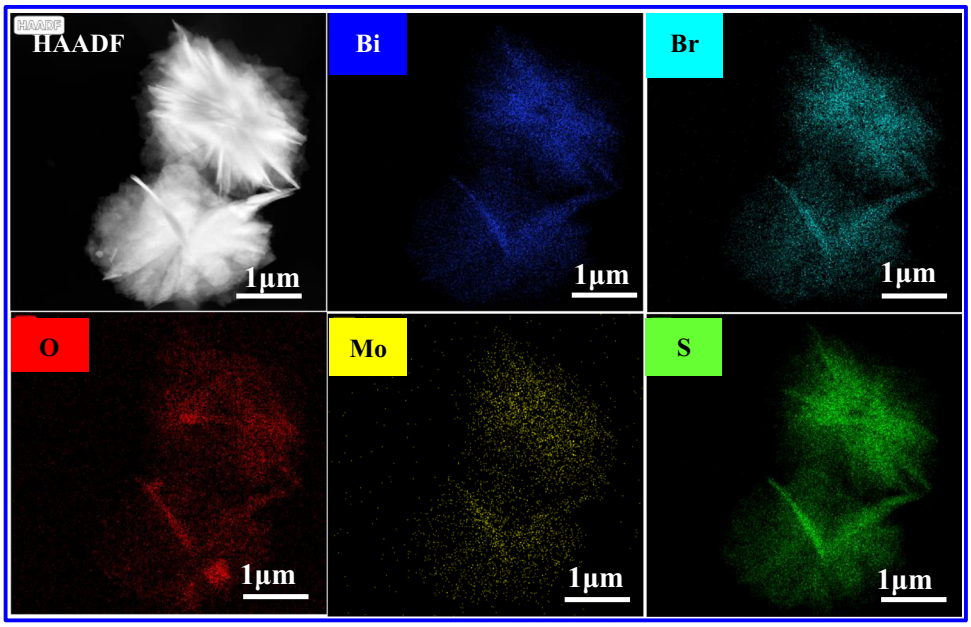

Fig. 3 Elemental distribution maps of 6-MoS_2/BiOBr composites

eV for 6-MoS_2/BiOBr heterojunctions. All these distinct shifts of Bi 4f, O 1s, and Br 3d orbits further proved the formation of heterojunction between MoS_2 and BiOBr in 6-MoS_2/BiOBr heterojunctions.

BET analysis

The Brunauer-Emmett-Teller (BET) surface area and porous structure of 6-MoS_2/BiOBr heterojunction and pure BiOBr are studied based on N_2 adsorption-desorption experiments, and the results are depicted in Fig. 5. It was clear that 6-MoS_2/BiOBr sample displayed type-II adsorption-desorption isotherms with H4 hysteresis loop (Fig. 5a), indicating the strong adsorption between 6-MoS_2/BiOBr and guest adsorbent. The pore size distribution was studied by the desorption data based on the Barrett-Joyner-Halenda (BJH) method. According to the inset in Fig. 5 a, 6-MoS_2/BiOBr heterojunction shows the mesoporous nature, and the formation of pores around 2–10 nm may be attributed to the crystal growth process or the gaps between assembled nanosheets which coincided with the SEM images. Pure BiOBr exhibited type IV isotherms with H3-type hysteresis loops (Fig. 5b), and the corresponding BJH analysis (inset in Fig. 5b) revealed that most of the pore sizes fell into the range from 2 to 16 nm. The BET surface areas of 6-MoS_2/BiOBr and pure BiOBr were about 54.9577 and 17.929 m^2/g, respectively. After introducing MoS_2 to BiOBr, the BET surface area of BiOBr was remarkably increased. It was beneficial for the adsorption of organic molecules and provided more active sites during the photocatalytic degradation process.

Photocatalytic degradation of tetracycline and levofloxacin

The photocatalytic capabilities of BiOBr and MoS_2/BiOBr heterostructures are investigated by photocatalytic removal of antibiotics tetracycline and levofloxacin aqueous solution, and the results are given in Fig. 6. As seen from Fig. 6 a and b, the degradation efficiency of tetracycline and levofloxacin in the existence of BiOBr are only about 69.99% and 66.08%, respectively. Remarkable enhancement of photocatalytic performance was obtained by the MoS_2/BiOBr heterojunctions. As shown, the photocatalytic activity of MoS_2/BiOBr heterojunctions dramatically depended on the coupling amount of MoS_2, and 6-MoS_2/BiOBr exhibited the best photocatalytic efficiency, 92.96% for tetracycline and 90.31% for levofloxacin within 70 min. Higher coupling of MoS_2 reduced the photocatalytic effect due to aggregation of MoS_2 particles and charge recombination (Zarezadeh et al. 2019). Figure 6 c and d show the dependence of UV-vis absorbance for tetracycline and levofloxacin in the absence and presence of heterojunctions. The intensity of major absorption peak for both tetracycline at 370 nm and levofloxacin at 287 nm gradually diminished with prolonging the illumination time and almost disappeared after 70 min, indicating the broken of molecular structure and the conjugated π system in the tetracycline and levofloxacin molecules. This result is very important for the practical antibiotics wastewater decontamination, since the 6-MoS_2/BiOBr heterojunctions displayed remarkable photocatalytic performance in the degradation of tetracycline and levofloxacin, the major effluents from therapeutic medicine, feed supplements, and pharmaceutical factory.

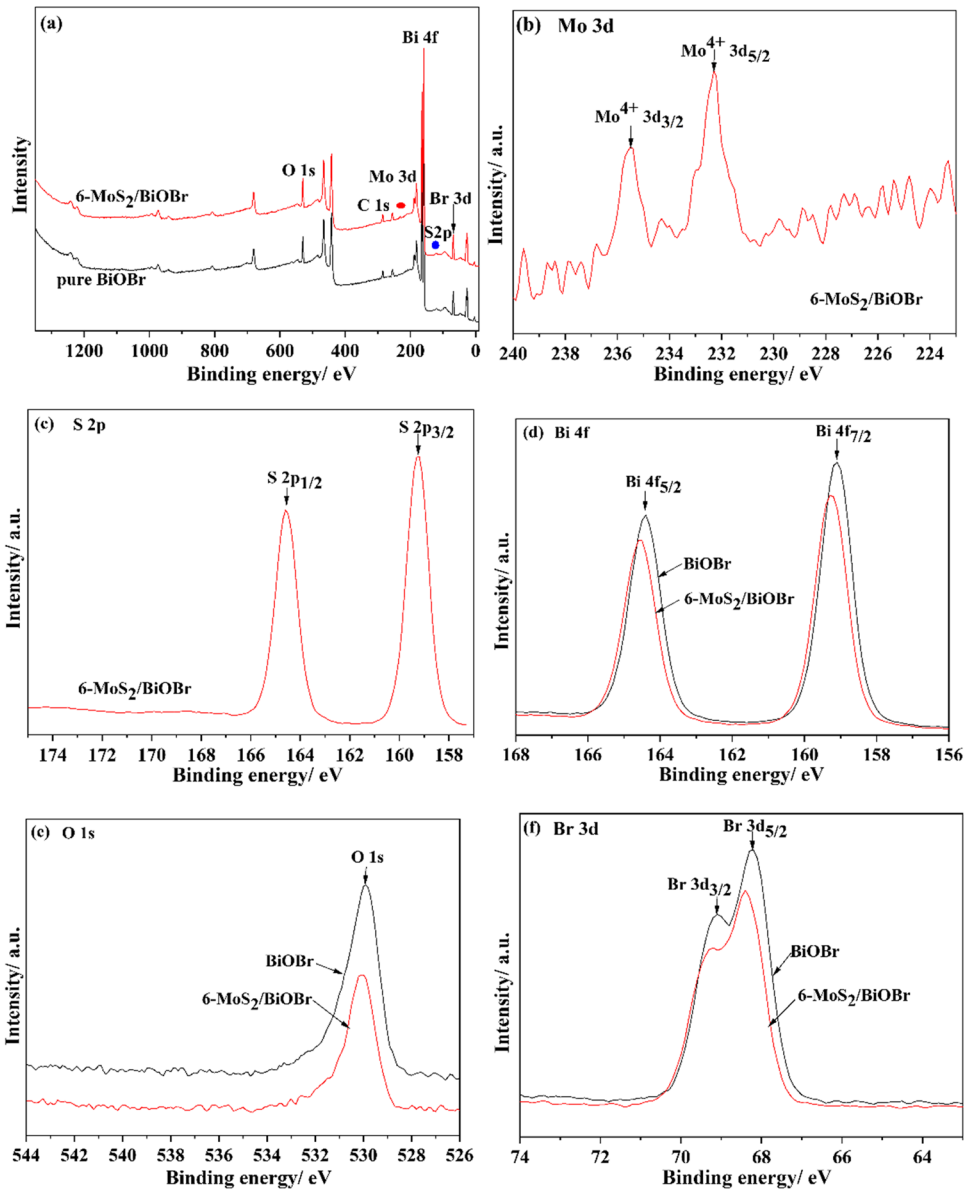

Fig. 4 XPS spectra of BiOBr and 6-MoS_2/BiOBr heterojunction **a** full spectra, **b** Mo 3d, **c** S 2p, **d** Bi 4f, **e** O 1s, and **f** Br 3d

Long-term stability of the photocatalysts is significant for the actual applications. To evaluate the durability of 6-MoS_2/BiOBr heterojunctions, the recycling degradation experiments for both tetracycline and levofloxacin were examined. The detailed process was based on our reported reference (Ma et al. 2019a). Typically, 6-MoS_2/BiOBr composites were collected by centrifugation after each run and washed with deionized water and recycled to another run. The experimental results are shown in Fig. 7. It was clear that the degradation efficiency of 6-MoS_2/BiOBr exhibited high stability and potential applications for eliminating antibiotics pollutants, since 85% of tetracycline and 81% of levofloxacin could still be efficiently degraded after 3 runs.

In addition, in order to ensure the mineralization of the pollutants, the mineralization efficiency of 6-MoS_2/BiOBr composites for both tetracycline and levofloxacin during the degradation reactions was monitored on an analytic Jena TOC analyzer (multi N/C 3100, Germany). From the TOC experimental data as listed in Table 1, the TOC elimination efficiencies for tetracycline and levofloxacin increase gradually with the reaction time, and nearly 55.06% of tetracycline and 63.28% of levofloxacin is mineralized within 4 h.

To investigate the migration, transfer, and separation properties of photo-generated electron/hole (e^-/h^+) pairs during the photocatalytic process in the presence of BiOBr and 6-MoS_2/BiOBr, the UV-vis diffuse reflectance spectra (DRS), photoluminescence (PL) spectroscopy, electrochemical impedance Nyquist (EIS), and transient photocurrent were employed. As evidenced in Fig. 8 a, the incorporation of MoS_2 displays a synergistic effect with significantly

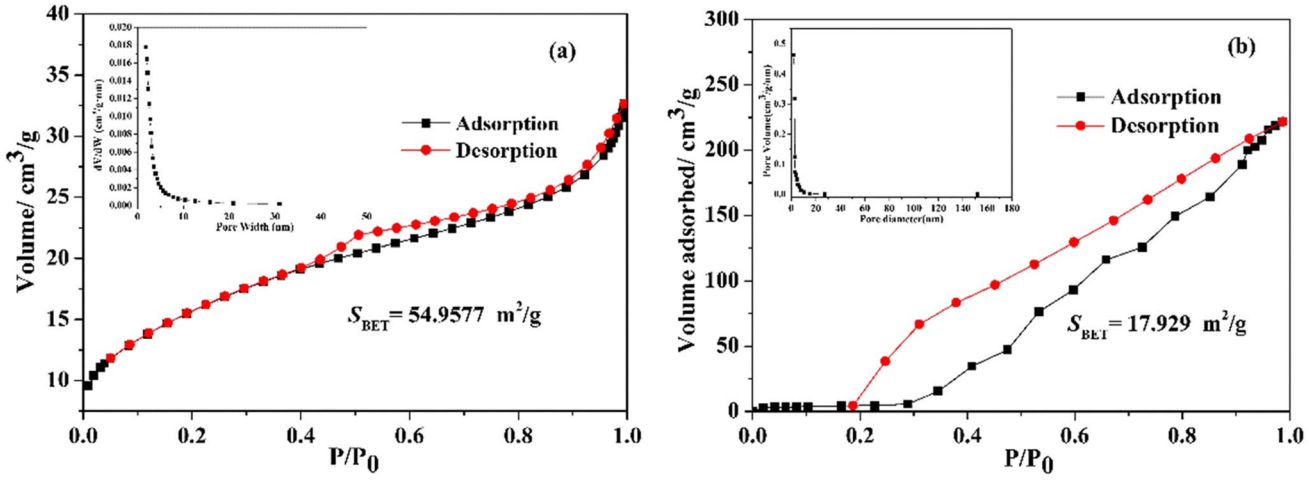

Fig. 5 Nitrogrn adsorption-desorption isotherms and corresponding pore-size distribution (inset figure) of 6-MoS2/BiOBr (**a**) and pure BiOBr (**b**)

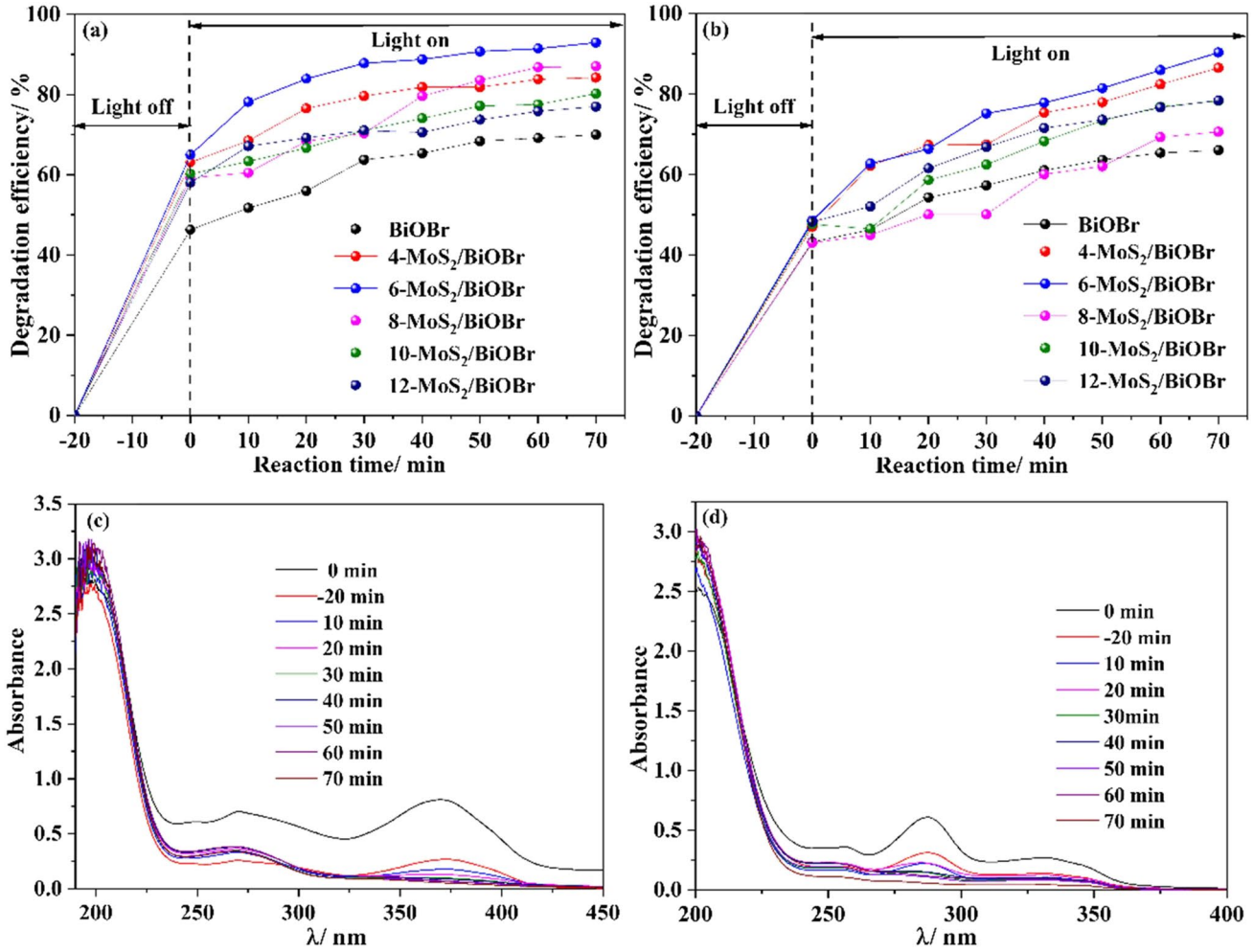

Fig. 6 Decomposition of tetracycline (**a**) and levofloxacin (**c**) under Xe lamp irradiation by BiOBr and MoS_2/BiOBr heterojunctions and UV-vis absorption spectra of tetracycline (**b**) and levofloxacin (**d**) during the photocatalytic degradation process by 6-MoS_2/BiOBr heterojunctions

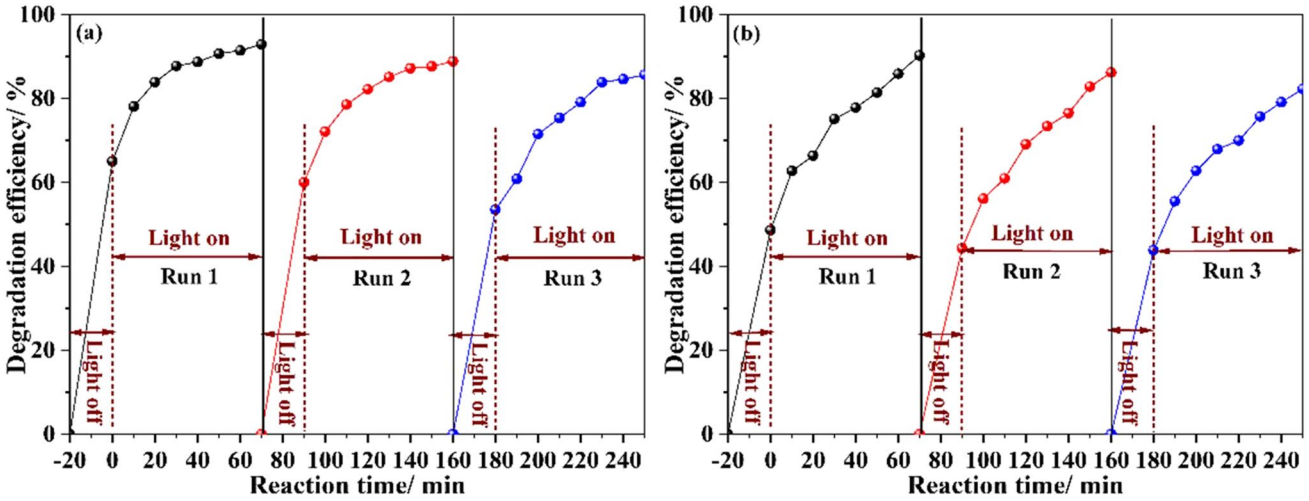

Fig. 7 Recycling experiments by 6-MoS2/BiOBr under visible light irradiation (**a**) tetracycline, and (**b**) levofloxacin

Table 1 Total carbon (TC, $mg{\cdot}L^{-1}$), total inorganic carbon (IC, $mg{\cdot}L^{-1}$), TOC ($mg{\cdot}L^{-1}$), and mineralization of tetracycline and solutions at different degradation times

Organics	Tetracycline				Levofloxacin			
Time	TC	IC	TOC	Min.%[a]	TC	IC	TOC	Min.%[a]
0	10.537	1.207	9.3428	0	10.279	1.542	8.455	0
1 h	9.231	0.644	8.1761	12.48	7.531	0.637	7.138	15.58
2 h	8.113	1.388	6.799	27.22	6.683	0.662	5.721	32.34
3 h	6.177	0.735	5.581	40.25	5.052	0.607	4.413	47.81
4 h	4.639	0.571	4.198	55.06	4.865	0.537	3.104	63.28

[a]Min. is the abbreviation of mineralization

improved visible light harvesting in the region of 400-600 nm for 6-MoS_2/BiOBr, in comparison with that of BiOBr. Furthermore, the PL intensity (Fig. 8b) and the EIS Nyquist radius (Fig. 8c) of 6-MoS_2/BiOBr dramatically decreased, compared with that of BiOBr, implying that the recombination of e^-/h^+ pairs in 6-MoS_2/BiOBr was strongly inhibited (Wu et al. 2020). The transient photocurrent shown in Fig. 8 d displays that BiOBr has a weak response signal, while the heterojunction 6-MoS_2-BiOBr exhibits stronger photocurrent than BiOBr, further proving that the efficient separation of photocarriers in 6-MoS_2/BiOBr is promoted. The above PL, EIS, and photocurrent results were in accordance with the previous photocatalytic performance.

Detection of reactive species

To specify the main reactive species involved in tetracycline and levofloxacin photo-degradation by 6-MoS_2/BiOBr, reactive radical capture experiments were conducted and ethylene di-ammine tetra acetic acid disodium (Na_2EDTA), isopropanol (IPA), and benzoquinone (BQ) were employed to capture h^+, ·H, and $\cdot O_2^-$, respectively. From Fig. 9 a, it could be seen that the degradation efficiency of tetracycline is dramatically suppressed from 92.96 to 54.78 and 63.23% with the addition of Na_2EDTA and IPA in tetracycline degradation process. However, the addition of BQ had a negligible effect on tetracycline degradation. This phenomenon depicted that h^+ and ·OH were the main reactive reagents in tetracycline degradation, and the same results were observed in levofloxacin degradation (Fig. 9b).

Mechanism of enhanced photocatalytic performance

A possible enhanced photocatalytic mechanism for tetracycline and levofloxacin degradation over MoS_2/BiOBr heterojunctions was proposed. Based on our previous work, the conduction band potential (E_{CB}) and valence band potential (E_{VB}) for MoS_2 is 0.33 and 1.33 eV (Ma et al. 2019b), whereas it is 0.19 and 3.17 eV for BiOBr (Ma et al. 2019a). The schematic diagram of energy band structure for MoS_2 and BiOBr is constructed and depicted in Fig. 10 a. As a p-type semiconductor, the Femi level of both MoS_2 and BiOBr are close to the valence band, and MoS_2 has a higher Femi level than BiOBr in the detached state. When MoS_2 and BiOBr were in contact (Fig. 10b), a p-p isotype

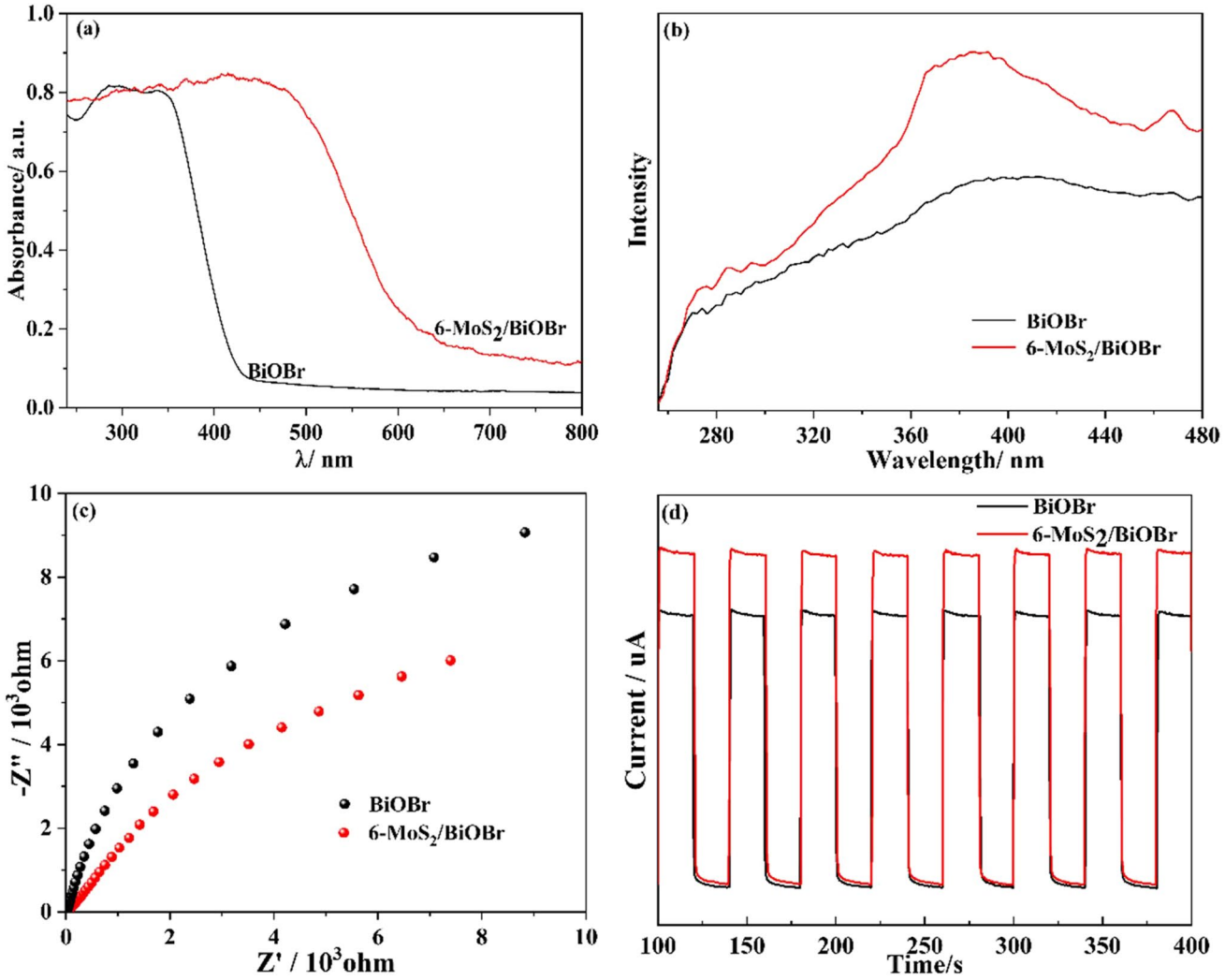

Fig. 8 UV-vis diffuse reflectance spectra (**a**), the photoluminescence spectroscopy (**b**), electrochemical impedance Nyquist (**c**), and transient photocurrent (**d**) curves of BiOBr and 6-MoS_2/BiOBr

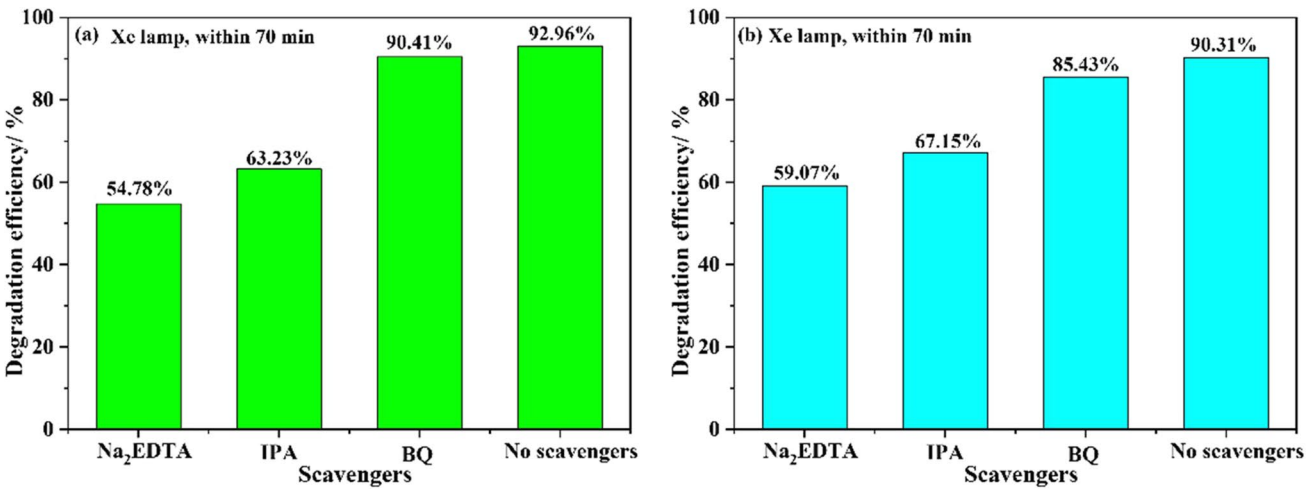

Fig. 9 The degradation efficiency of tetracycline (**a**) and levofloxacin (**b**) over the 6-MoS_2/BiOBr heterojunctions in the presence of scavengers

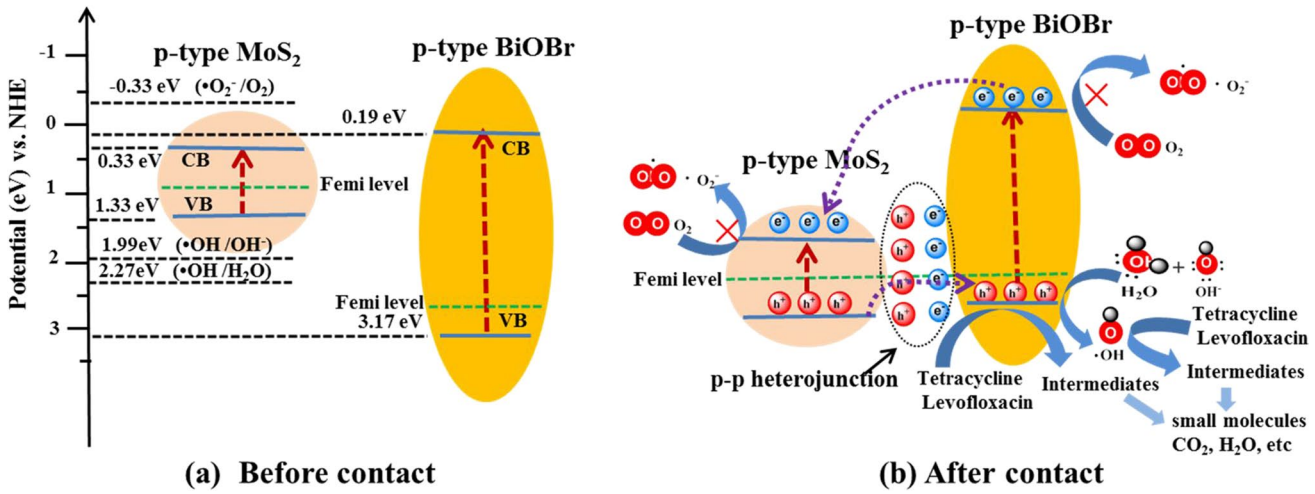

Fig. 10 The proposed mechanism of enhanced photocatalytic performance over MoS_2/BiOBr heterojunctions

heterojunction was produced. The difference in Femi levels between MoS_2 and BiOBr led to the transfer of photo-generated holes from MoS_2 to BiOBr until the Femi level of two components reached an equilibrium, producing a hole accumulation region at MoS_2 and a hole depletion region at BiOBr (Zhang et al. 2020). Accompanied with the moving of Femi level, the whole energy band of BiOBr was elevated, while that of MoS_2 was descended. Thus, an inner electric field from MoS_2 to BiOBr was established at the interface. As irradiated by the visible-light, both MoS_2 and BiOBr could absorb photons and induce the generation of electron/hole pairs. Driven by the inner electric field, the photo-generated electrons on CB of BiOBr are rapidly migrated to that of MoS_2, and the holes on VB of MoS_2 are transferred to that of BiOBr. Thus, the separation of electron/hole pairs in BiOBr was promoted, and accordingly their recombination was reduced. The more efficient separation of electron/hole pairs could reduce the total voltage barrier at the interface, resulting in lower resistance and higher photocurrent, in agreement with the results in Fig. 8 c and d.

Since E_{CB} of both MoS_2 and BiOBr were more positive than the oxidation potential of $O_2/\cdot O_2^-$ (−0.33 eV vs NHE (Liu et al. 2022; Liu et al. 2017). So $\cdot O_2^-$ radicals cannot be produced by both MoS_2 and BiOBr, which had been confirmed by the radical capturing experiments (Fig. 10). The E_{VB} of MoS_2 was lower than that of the reduction potential of $\cdot OH/OH^-$ (1.99 eV vs NHE and $\cdot OH/H_2O$ (2.27 V vs NHE (Li et al. 2018). While the BiOBr had a more positive E_{VB} value than 1.99 and 2.27 eV, so the OH^- or H_2O could be oxidized to ·OH radicals by BiOBr but not by MoS_2. The ·OH radicals possess strong oxidation ability and could degrade organic molecules to small molecules. The participation of ·OH radicals in the degradation process had been approved by radical capturing experiments (Fig. 9).

In a word, the fabrication of p-p heterojunction structure at the interface of MoS_2 and BiOBr facilitates the transfer and separation of photo-generated e^-/h^+ pairs, which could be confirmed by the diminished PL intensity, the decreased EIS Nyquist radius, and increased photocurrent signal shown in Fig. 8. The reaction procedure involved in the photo-degradation of tetracycline, and levofloxacin was depicted with the following equations:

$$MoS_2/BiOBr + h\nu \rightarrow MoS_2\ (e^-) + Bi_2O_3\ (h^+) + MoS_2\ (h^+) + BiOBr\ (h^+) \quad (1)$$

$$h^+\ (BiOBr) + H_2O \rightarrow \cdot OH + H^+ \quad (2)$$

$$h^+\ (BiOBr) + OH^- \rightarrow \cdot OH \quad (3)$$

$$\cdot OH + \text{tetracycline or levofloxacin} \rightarrow \text{intermediates} \rightarrow CO_2 + H_2O \quad (4)$$

$$h^+ + \text{tetracycline or levofloxacin} \rightarrow \text{intermediates} \rightarrow CO_2 + H_2O \quad (5)$$

Conclusion

In this paper, 3D sheet-packed hierarchical MoS_2/BiOBr p-p heterojunctions were fabricated via a simple deposition-hydrothermal method. In comparison with pure BiOBr, the MoS_2/BiOBr heterojunctions demonstrated enhanced photocatalytic capability in removal of tetracycline and levofloxacin. The enhanced photocatalytic ability could be accredited to the synergistic effect of stronger photo-absorption and the fabrication of p-p heterojunction at the interface of MoS_2 and BiOBr, which facilitated the separation and migration of

photo-induced e^-/h^+ pairs. Photo-generated holes and ·OH radicals acted as a key role in the whole degradation process. This MoS_2/BiOBr heterojunction was a promising photocatalyst suitable for eliminating antibiotics in wastewater.

Availability of data and materials The datasets and materials used in study are available from the authors.

Authors' contributions Zhanying Ma: visualization and investigation. Yangqing He: conceptualization, methodology, writing — original draft, writing — review and editing, and supervision. Xiaobo Li, Guang Fan, and Lingjuan Deng: formal analysis. All the authors reviewed the manuscript.

Funding This work was supported by the key research and development (R&D) plan of Shaanxi Province (2023-YBSF-595) and the Natural Science Foundation of Shaanxi Province (2019JQ-221).

Declarations

Ethics approval and consent to participate Not applicable.

Consent for publication All the authors agreed to publish the paper upon acceptance.

Conflict of interest The authors declare no competing interests.

References

Akhundi A, Badiei A, Ziarani GM, Aziz H-Y, Muñoz-Batista MJ, Luque R (2020) Graphitic carbon nitride-based photocatalysts: toward efficient organic transformation for value-added chemicals production. Mol Catal 488:110902. https://doi.org/10.1016/j.mcat.2020.110902

Benavente E, Durán F, Sotomayor-Torres C, González G (2018) Heterostructured layered hybrid ZnO/MoS_2 nanosheets with enhanced visible light photocatalytic activity. J Phys Chem Solids 113:119–124. https://doi.org/10.1016/j.jpcs.2017.10.027

Chandrabose G, Dey A, Gaur SS, Pitchaimuthu S, Jagadeesan H, St John Braithwaite N, Selvaraj V, Kumar V, Krishnamurthy S (2021) Removal and degradation of mixed dye pollutants by integrated adsorption-photocatalysis technique using 2-D MoS_2/TiO_2 nanocomposite. Chemosphere 279:130467. https://doi.org/10.1016/j.chemosphere.2021.130467

Chen DY, Li BL, Pu QM, Chen X, Wen G, Li ZS (2019) Preparation of Ag-$AgVO_3$ /g-C_3N_4 composite photo-catalyst and degradation characteristics of antibiotics. J Hazard Mater 373:303–312. https://doi.org/10.1016/j.jhazmat.2019.03.090

Darsara SA, Seifi M, Askari MB (2018) One-step hydrothermal synthesis of MoS_2/CdS nanocomposite and study of structural, photocatalytic, and optical properties of this nanocomposite. Optik 169:249–256. https://doi.org/10.1016/j.ijleo.2018.05.075

Hu XY, Zeng XK, Liu Y, Lu J, Yuan S, Yin YC, Hu J, McCarthy DT, Zhang XW (2020) Nano-layer based 1T-rich MoS_2/g-C_3N_4 co-catalyst system for enhanced photocatalytic and photoelectrochemical activity. Appl Catal B Environ 268:118466. https://doi.org/10.1016/j.apcatb.2019.118466

Hu Z, Ge M, Guo CS (2021) Efficient removal of levofloxacin from different water matrices via simultaneous adsorption and photocatalysis using a magnetic Ag_3PO_4/rGO/$CoFe_2O_4$ catalyst. Chemosphere 268:128834. https://doi.org/10.1016/j.chemosphere.2020.128834

Iqbal M, Ibrar A, Ali A, Hussain S, Shad S, Ullah S, Alshahrani T, Hakami J, Khan F, Thebo KH (2022) Facile synthesis of Mn doped Bi_2S_3 photocatalyst for efficient degradation of organic dye under visible-light irradiation. J Mol Struct 1267:133598. https://doi.org/10.1016/j.molstruc.2022.133598

Lee WPC, Wong FH, Attenborough NK, Kong XY, Tan LL, Sumathi S, Chai SP (2017) Two-dimensional bismuth oxybromide coupled with molybdenum disulphide for enhanced dye degradation using low power energy-saving light bulb. J Environ Manag 197:63–69. https://doi.org/10.1016/j.jenvman.2017.03.027

Li MF, Liu YG, Zeng GM, Liu N, Liu SB (2019a) Graphene and graphene-based nanocomposites used for antibiotics removal in water treatment: a review. Chemosphere 226:360–380. https://doi.org/10.1016/j.chemosphere.2019.03.117

Li N, Zhou J, Sheng Z, Xiao W (2018) Molten salt-mediated formation of g-C_3N_4-MoS_2 for visible-light-driven photocatalytic hydrogen evolution. Appl Surf Sci 430:218–224. https://doi.org/10.1016/j.apsusc.2017.08.086

Li WB, Wang L, Zhang Q, Chen ZY, Deng XY, Feng C, Xu LK, Sun MX (2019b) Fabrication of an ultrathin 2D/2D C_3N_4/MoS_2 heterojunction photocatalyst with enhanced photocatalytic performance. J Alloys Compd 808:151681. https://doi.org/10.1016/j.jallcom.2019.151681

Li WX, Li XC, Fu XH, Lou ZZ, Zhu Y, Zhang YM (2023) Photo-induced conversion of type-II CoPc/BiOBr-NSs to S-scheme heterostructure for boosting CO_2 photoreduction. Chem Eng J 51:138932

Liao HR, Zhong JB, Li JZ, Huang ST, Duan R (2021) Photocatalytic properties of flower-like BiOBr/BiOCl heterojunctions in-situ constructed by a reactable ionic liquid. Inorg Chem Commun 134:109063

Liu C, Wu QS, Ji MW, Zhu HJ, Hou HJ, Yang QH, Jiang CF, Wang JJ, Tian L, Chen J, Hou WH (2017) Constructing Z-scheme charge separation in 2D layered porous BiOBr/graphic C_3N_4 nanosheets nonojunction with enhanced photocatalytic activity. J Alloys Compd 723:1121–1131

Liu HJ, Wang BJ, Chen M, Zhang H, Peng JB, Ding L, Wang WF (2021) Simple synthesis of BiOAc/BiOBr heterojunction composites for the efficient photocatalytic removal of organic pollutants. Sep Purif Technol 261:118286

Liu YL, He JY, Qi Y, Wang YW, Long F, Wang M (2022) Preparation of flower-like BiOBr/Bi_2WO_6 Z-scheme heterojunction through an ion exchange process with enhanced photocatalytic activity. Mater Sci Semicond Process 137:106195

Liu YZ, Zhang HY, Ke J, Zhang JQ, Tian WJ, Xu XY, Duan XG, Sun HQ, Tade MO, Wang SB (2018) 0D (MoS_2)/2D (g-C_3N_4) heterojunctions in Z-scheme for enhanced photocatalytic and electrochemical hydrogen evolution. Appl Catal B Environ 228:64–74

Lu C, Wu WD, Zhou HF (2021) In situ fabrication of BiOBr/$BiFeWO_6$ heterojunction with excellent photodegradation activity under visible light. J Solid State Chem 303:122465

Ma ZY, Deng LJ, Fan G, He YQ (2019a) Hydrothermal synthesis of p-C_3N_4/f-BiOBr composites with highly efficient degradation of methylene blue and tetracycline. Spectrochim Acta A 214:103–110

Ma ZY, Hu LL, Li XB, Deng LJ, Fan G, He YQ (2019b) A novel nano-sized MoS_2 decorated Bi_2O_3 heterojunction with enhanced photocatalytic performance for methylene blue and tetracycline degradation. Ceram Int 45:15824–15833. https://doi.org/10.1016/j.ceramint.2019.05.085

Mao DJ, Lü XM, Jiang ZF, Xie JM, Lu XF, Wei W, Hossain AMS (2014) Ionic liquid-assisted hydrothermal synthesis of square BiOBr nanoplates with highly efficient photocatalytic activity. Mater Lett 118:154–157. https://doi.org/10.1016/j.matlet.2013.12.049

Meng XC, Zhang ZS (2015) Facile synthesis of BiOBr/Bi_2WO_6 heterojunction semiconductors with high visible-light-driven photocatalytic activity. J Photoch Photobio A 310:33–44. https://doi.org/10.1016/j.jphotochem.2015.04.024

Pirhashemi M, Habibi-Yangjeh A, Pouran SR (2018) Review on the criteria anticipated for the fabrication of highly efficient ZnO-based visible-light-driven photocatalysts. J Ind Eng Chem 62:1–25. https://doi.org/10.1016/j.jiec.2018.01.012

Sabri M, Habibi-Yangjeh A, Pouran SR, Wang CD (2021) Titania-activated persulfate for environmental remediation: the-state-of-the-art. Catal Rev. https://doi.org/10.1080/01614940.2021.1996776

Van ND, Huong NT, Le NTH, Nam MH (2022) One-pot synthesis of $BiSbO_4$/BiOBr nanocomposite with excellent UV-photocatalytic activity. Ceram Int 48:8715–8720. https://doi.org/10.1016/j.ceramint.2021.12.022

Wang J, Dong C, Jiang BB, Wu KL, Sun J, Li XZ, Zhang WJ, Zhang B, Wei XW (2014) Preparation of visible light-driven Ag_2CO_3/BiOBr composite photocatalysts with universal degradation abilities. Mater Lett 131:108–111

Wu J, Xie Y, Ling Y, Si JC, Li X, Wang JL, Ye H, Zhao JS, Li SQ, Zhao QD, Hou Y (2020) One-step synthesis and Gd^{3+} decoration of BiOBr microspheres consisting of nanosheets toward improving photocatalytic reduction of CO_2 into hydrocarbon fuel. Chem Eng J 400:125944. https://doi.org/10.1016/j.matlet.2014.05.153

Xiong JY, Dong QS, Wang T, Jiao ZB, Lu GX, Bi YP (2014) Direct conversion of Bi nanospheres into 3D flower-like BiOBr nanoarchitectures with enhanced photocatalytic properties. RSC Adv 4:583–586. https://doi.org/10.1039/C3RA46088F

Xu ZK, Han L, Lou BH, Zhang XW, Dong SJ (2014) High-performance BiOBr ultraviolet photodetector fabricated by a green and facile interfacial self-assembly strategy. Nanoscale 6:145–150. https://doi.org/10.1039/C3NR04496C

Xue C, Xia JL, Wang T, Zhao SS, Yang GD, Yang BL, Dai YZ, Yang G (2014) A facile and efficient solvothermal fabrication of three-dimensionally hierarchical BiOBr microspheres with exceptional photocatalytic activity. Mater Lett 133:274–277. https://doi.org/10.1016/j.matlet.2014.07.016

Zarezadeh S, Habibi-Yangjeh A, Mousavi M (2019) Fabrication of novel ZnO/BiOBr/C-Dots nanocomposites with considerable photocatalytic performances in removal of organic pollutants under visible light. Adv Powder Technol 301:197–1209. https://doi.org/10.1016/j.apt.2019.03.016

Zhang BF, Zhang MT, Zhang L, Bingham PA, Tanaka M, Li W, Kubuki S (2021) BiOBr/MoS_2 catalyst as heterogenous peroxymonosulfate activator toward organic pollutant removal: energy band alignment and mechanism insight. J Colloid Interface Sci 594:635–649. https://doi.org/10.1016/j.jcis.2021.03.066

Zhang Y, Wang Q, Liu DM, Wang Q, Li T, Wang Z (2020) Cu_2O-BiOI isotype (p-p) heterojunction: boosted visible-light-driven photoelectrochemical activity for non-enzymatic H_2O_2 sensing. Appl Surf Sci 521:146434. https://doi.org/10.1016/j.apsusc.2020.146434